

Article

## Synthesis, Characterization and Photocatalytic Activity of New Photocatalyst ZnBiSbO<sub>4</sub> under Visible Light Irradiation

Jingfei Luan \*, Mengjing Chen and Wenhua Hu

State Key Laboratory of Pollution Control and Resource Reuse, School of the Environment, Nanjing University, Nanjing 210093, China; E-Mails: custcmj@gmail.com (M.C.); wenhuahu2000@163.com (W.H.)

\* Author to whom correspondence should be addressed; E-Mail: jfluan@nju.edu.cn; Tel./Fax: +86-25-8370-7304.

Received: 9 March 2014; in revised form: 9 May 2014 / Accepted: 16 May 2014 /

Published: 28 May 2014

---

**Abstract:** In this paper, ZnBiSbO<sub>4</sub> was synthesized by a solid-state reaction method for the first time. The structural and photocatalytic properties of ZnBiSbO<sub>4</sub> had been characterized by X-ray diffraction, scanning electron microscopy, X-ray photoelectron spectroscopy, Fourier-transform infrared spectroscopy, transmission electron microscope and UV-visible spectrometer. ZnBiSbO<sub>4</sub> crystallized with a pyrochlore-type structure and a tetragonal crystal system. The band gap of ZnBiSbO<sub>4</sub> was estimated to be 2.49 eV. The photocatalytic degradation of indigo carmine was realized under visible light irradiation with ZnBiSbO<sub>4</sub> as a catalyst compared with nitrogen-doped TiO<sub>2</sub> (N-TiO<sub>2</sub>) and CdBiYO<sub>4</sub>. The results showed that ZnBiSbO<sub>4</sub> owned higher photocatalytic activity compared with N-TiO<sub>2</sub> or CdBiYO<sub>4</sub> for the photocatalytic degradation of indigo carmine under visible light irradiation. The reduction of the total organic carbon, the formation of inorganic products, SO<sub>4</sub><sup>2-</sup> and NO<sub>3</sub><sup>-</sup>, and the evolution of CO<sub>2</sub> revealed the continuous mineralization of indigo carmine during the photocatalytic process. One possible photocatalytic degradation pathway of indigo carmine was obtained. The phytotoxicity of the photocatalytic-treated indigo carmine (IC) wastewater was detected by examining its effect on seed germination and growth.

**Keywords:** ZnBiSbO<sub>4</sub>; indigo carmine; photocatalytic degradation; visible light irradiation; photodegradation pathway

---

## 1. Introduction

Dye effluents from textile industries and photographic industries are becoming a serious environmental problem because of their toxicity, unacceptable color, high chemical oxygen demand content and biological degradation [1]. The presence of dye in water is not only aesthetically displeasing, but also affects water transparency, which results in the reduction of sunlight penetration, gas solubility and the photosynthetic reaction [2]. In order to solve this problem, many scientists look forward to degrading harmful dye effluents from contaminated water with photocatalytic techniques before appropriate disposal, and these scientists have been contributing their various efforts to this career for more than 40 years [3–5]. Nowadays, photocatalytic degradation processes have been widely applied as techniques for the destruction of organic pollutants in wastewater and effluents, especially the degradation of dyes [6].

The choice of the wavelength of incident light is important for a photocatalytic degradation system, because light was the source of energy. Previous studies have shown that such semiconductor compounds could degrade most kinds of persistent organic pollutants, such as dyes, pesticide, detergents and volatile organic compounds, under UV-light irradiation [7–10], which has a higher energy than visible light. As is well known, ultraviolet light occupies only 4% of sunlight; on the other hand, visible light accounts for a share of about 43%. Thus, it seems more practical and favorable to use visible light rather than ultraviolet light for the degradation process. Therefore, it is necessary and urgent to make substantive efforts to develop new photocatalysts, which have a response to visible light and show a relatively high efficiency of degradation. In general, the majority of visible light-driven catalysts in previous research could mainly be classified into two types: one kind is called the TiO<sub>2</sub>-based catalyst, whose maximum absorption wavelength had been extended to visible light by ion doping [11–20] and cocatalyst recombination [21–31]; the other one is a multiple complex oxide, such as BiVO<sub>4</sub>, Bi<sub>12</sub>TiO<sub>20</sub>, K<sub>6</sub>Nb<sub>10.8</sub>O<sub>30</sub>, *etc.* [32–38]. Recently, a spinel type oxide with a formula of AB<sub>2</sub>O<sub>4</sub> had been found to perform excellent for degrading dyes that existed in wastewater under visible light irradiation. For example, MIn<sub>2</sub>O<sub>4</sub> (M = Ca, Sr, Ba) [11,39,40], NiCo<sub>2</sub>O<sub>4</sub> [11] and ZnFe<sub>2</sub>O<sub>4</sub>/MWCNTs [41] were synthesized for methylene blue degradation under visible light irradiation. Additionally, ZnFe<sub>2</sub>O<sub>4</sub> [42] was also reported to perform outstandingly for methyl orange degradation under visible light irradiation.

In this paper, newly synthesized semiconductor catalyst ZnBiSbO<sub>4</sub> which belongs to the AB<sub>2</sub>O<sub>4</sub> compound family is presented. We choose indigo carmine (IC) as the model pollutant to evaluate the degradation activity of ZnBiSbO<sub>4</sub> under visible light irradiation, because indigo carmine is widely applied and difficult for biodegradation. Additionally, the structural and photocatalytic properties of ZnBiSbO<sub>4</sub> have been investigated in detail. For comparison, we select N-TiO<sub>2</sub>, one kind of traditional photocatalyst, as a catalyst for IC under visible light irradiation. Besides, comparative experiments have been conducted by using CdBiYO<sub>4</sub> [43], one representative catalyst of the AB<sub>2</sub>O<sub>4</sub>-type compounds, which has been published in our former work, to demonstrate further the superiority of the degradation activity of ZnBiSbO<sub>4</sub>.

## 2. Results and Discussion

### 2.1. Crystal Structure and Optical Properties

The transmission electron microscopy (TEM) image of the prepared catalyst, ZnBiSbO<sub>4</sub>, is shown in Figure 1. It could be observed clearly from Figure 1a,b that the particles of ZnBiSbO<sub>4</sub> had a nanostructure and irregular shapes. Additionally, we could also acknowledge that the particles of ZnBiSbO<sub>4</sub> crystallized well, and the average particle size was about 220 nm in diameter. Figure 1b also shows the selected area electron diffraction pattern of ZnBiSbO<sub>4</sub>. It could be seen from Figure 1b that ZnBiSbO<sub>4</sub> crystallized with a pyrochlore-type structure, a tetragonal crystal system and a space group I41/A, and the lattice parameters for ZnBiSbO<sub>4</sub> were proven to be  $a = b = 12.040078 \text{ \AA}$  and  $c = 10.731416 \text{ \AA}$ . According to the calculation results from Figure 1b, the  $(h k l)$  value for the main peaks of ZnBiSbO<sub>4</sub> could be found and indexed. The histogram of the size distribution of ZnBiSbO<sub>4</sub> was also demonstrated in Figure 1c, and we could find that the particle size of the majority of ZnBiSbO<sub>4</sub> was from 170 to 270 nm. Brunauer–Emmett–Teller (BET) measurements were also detected, and the specific surface area of ZnBiSbO<sub>4</sub> was  $2.87 \text{ m}^2 \cdot \text{g}^{-1}$ .

**Figure 1.** (a) transmission electron microscopy (TEM) image of ZnBiSbO<sub>4</sub>; and (b) The selected area electron diffraction pattern of ZnBiSbO<sub>4</sub>; and (c) histogram of the size distribution of ZnBiSbO<sub>4</sub> calcinated at 800 °C for 35 h.

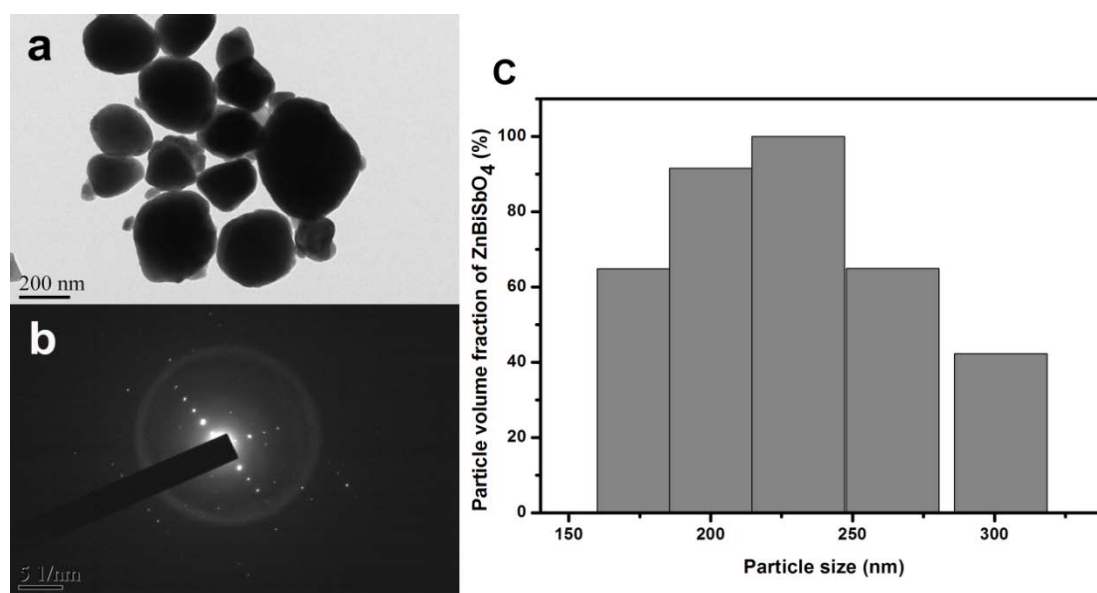
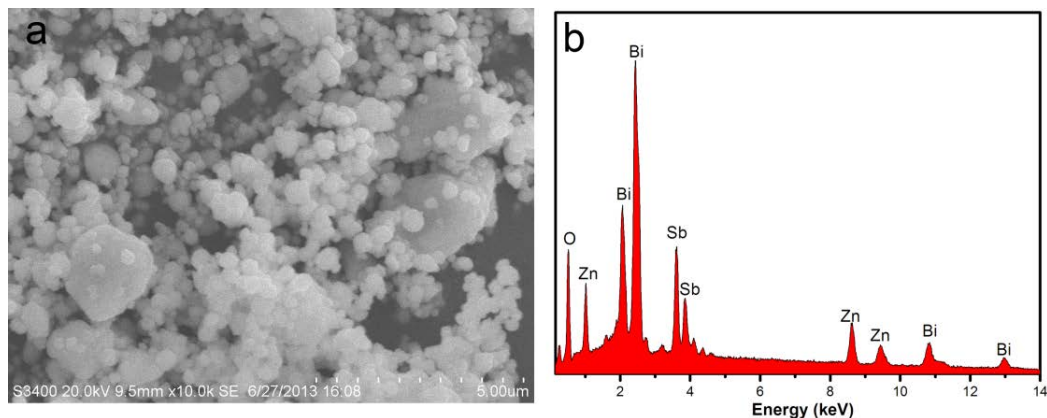


Figure 2 presents the scanning electron microscopy-energy-dispersive spectrometry (SEM-EDS) spectrum of ZnBiSbO<sub>4</sub>, indicating the presence of zinc, bismuth, antimony and oxygen element. In order to avoid the influence of inhomogeneity phenomenon on the selected surface, ten different specimen areas selection of ZnBiSbO<sub>4</sub> were conducted in an EDS test. The mean of the results of the above EDS spectra taken from prepared ZnBiSbO<sub>4</sub> indicated that the stoichiometric ratio of zinc, bismuth, antimony and oxygen was estimated to be 14.83:14.55:13.56:57.06, namely 1.05:1.03:0.96:4.04.

**Figure 2.** (a) scanning electron microscopy (SEM) spectrum of ZnBiSbO<sub>4</sub>; (b) energy-dispersive spectrometry (EDS) spectrum of ZnBiSbO<sub>4</sub> calcinated at 800 °C for 35 h.



In order to get a better understanding of the chemical state of all elements on the catalyst surface, the X-ray photoelectron spectroscopy (XPS) full spectrum of ZnBiSbO<sub>4</sub> was measured and is displayed in Figure 3. The atom XPS spectra of Zn, Bi and Sb are shown in Figure 4a–c, respectively. As to the O atom XPS spectrum, we could observe that the O 1s peak was asymmetric and should be overlaid by the Sb 3d<sub>5/2</sub> peak and the O 1s peak. Besides lattice oxygen (O<sub>I</sub>) in multiple oxide catalyst, the existence of chemisorbed oxygen (O<sub>II</sub>) on the surface of the catalyst should also be taken into consideration [44]. Thus, the fitted curves of Sb 3d<sub>5/2</sub> and O 1s for XPS spectra are given in Figure 4d, and the fitting results are reported in Table 1. The various elemental peaks, which correspond to the specific binding energies of ZnBiSbO<sub>4</sub>, are given in Table 2. The area ratio of O<sub>I</sub>/O<sub>T</sub> was 87.36% (O<sub>T</sub> contained O<sub>I</sub> and O<sub>II</sub>), meaning that the atom ratio of O<sub>I</sub>/O<sub>T</sub> is 87.36% on the catalyst surface. The results further suggested that the oxidation state of Zn, Bi, Sb and O ions from ZnBiSbO<sub>4</sub> were +2, +3, +3 and –2, respectively. After calculation with the reported method [45], the average atomic ratio of Zn:Bi:Sb:O for ZnBiSbO<sub>4</sub> was 1.00:0.98:1.02:4.12 based on our XPS results. The slight difference between the results that were found in XPS and EDS measurements could be ascribed to the inhomogeneity of different selected areas of ZnBiSbO<sub>4</sub> during the testing. Therefore, it could be deduced that the obtained material was of high purity under our preparation conditions.

**Figure 3.** The X-ray photoelectron spectroscopy (XPS) full spectrum of ZnBiSbO<sub>4</sub> calcinated at 800 °C for 35 h.

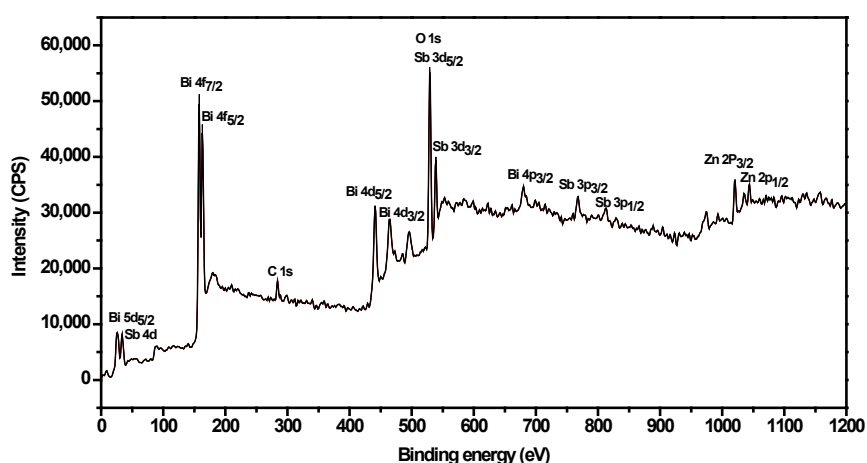


**Figure 4.** (a) The XPS spectrum of Zn 2p; (b) the XPS spectrum of Bi 4f; (c) the XPS spectrum of Sb 3d; and (d) peak curves of Sb 3d<sub>5/2</sub> and O 1s for the XPS spectrum of ZnBiSbO<sub>4</sub> (O<sub>I</sub>, lattice oxygen; O<sub>II</sub>, chemisorbed oxygen).

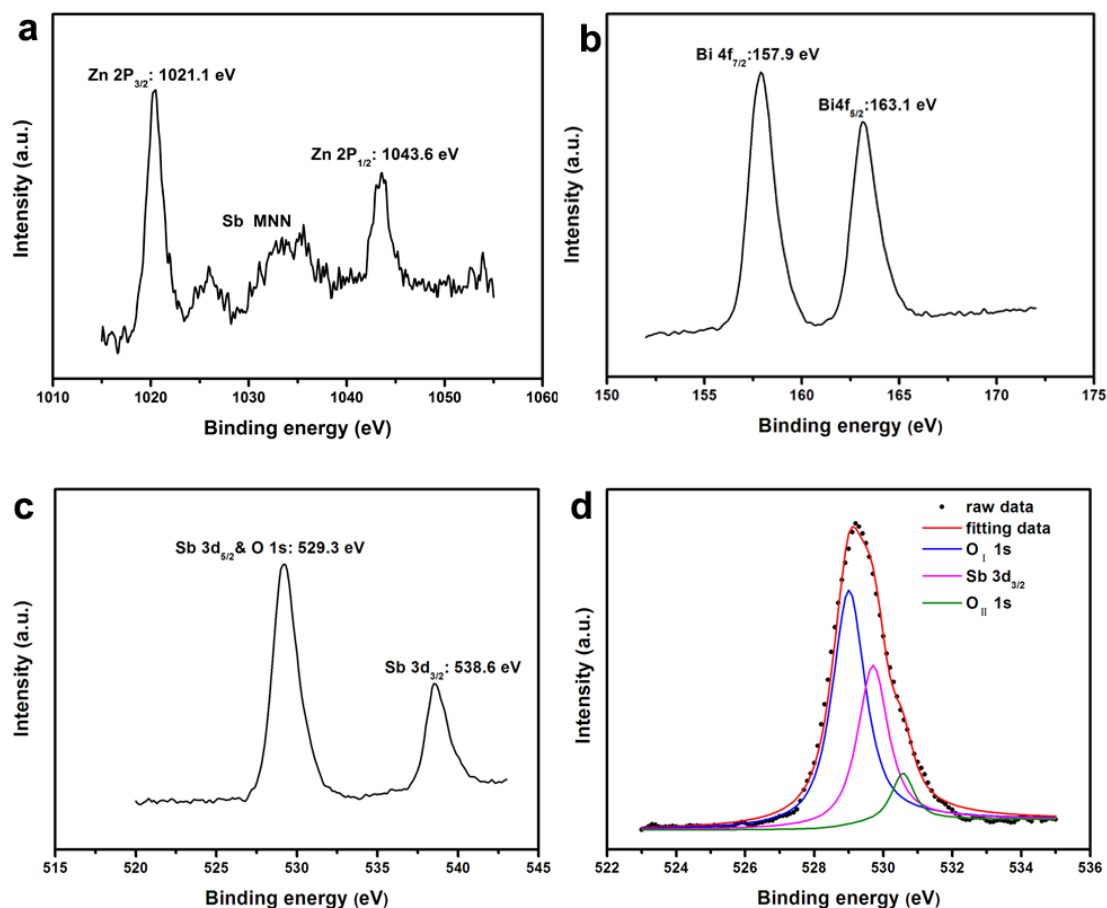


**Table 1.** XPS data corresponding to Figure 4d.

Element	Sb 3d <sub>5/2</sub>	O 1s	
		O <sub>I</sub>	O <sub>II</sub>
Binding energy (eV)	529.7	529.0	530.6

**Table 2.** Binding energies for key elements of ZnBiSbO<sub>4</sub>.

Element	Zn 2p <sub>3/2</sub>	Bi 4f <sub>7/2</sub>	Sb 3d <sub>5/2</sub>	O 1s
Binding energy (eV)	1021.1	157.9	529.7	529.0

Figure 5 shows the powder X-ray diffraction pattern of ZnBiSbO<sub>4</sub> with the full-profile structure refinements of the collected data, which were obtained by the RIETAN<sup>TM</sup> [46] program based on the Rietveld analysis. It could be seen from Figure 5 that ZnBiSbO<sub>4</sub> turned out to be a single phase. Additionally, the results of the final refinements for ZnBiSbO<sub>4</sub> indicated a good agreement between the observed intensities and calculated intensities for the pyrochlore-type structure, a tetragonal crystal system and a space group, I41/A (O atoms were included in the model). The lattice parameters for ZnBiSbO<sub>4</sub> were  $a = b = 12.040078 \text{ \AA}$  and  $c = 10.731416 \text{ \AA}$ . All the diffraction peaks for ZnBiSbO<sub>4</sub> could be successfully indexed according to the lattice constant and above space group. The atomic

coordinates and structural parameters of  $\text{ZnBiSbO}_4$  are listed in Table 3. According to above results, the structural model of  $\text{ZnBiSbO}_4$  which is simulated by Materials Studio software is demonstrated in Figure 6.

**Figure 5.** X-ray diffraction (XRD) pattern and Rietveld refinements of  $\text{ZnBiSbO}_4$ .

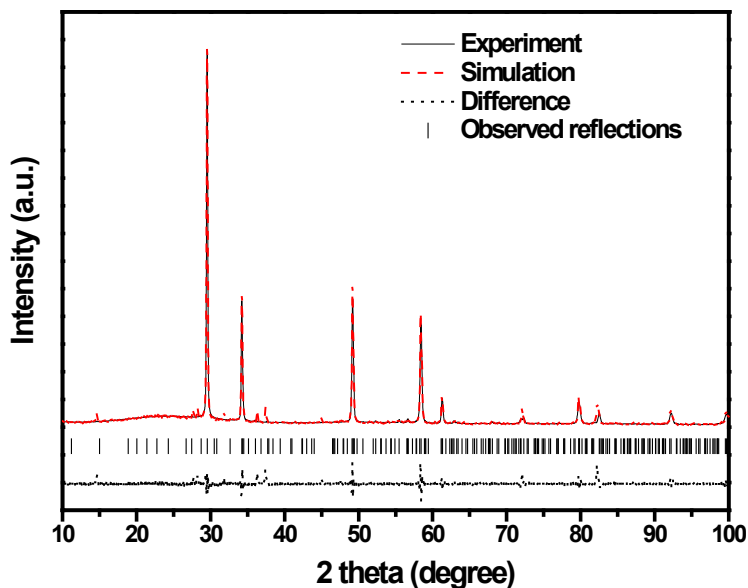
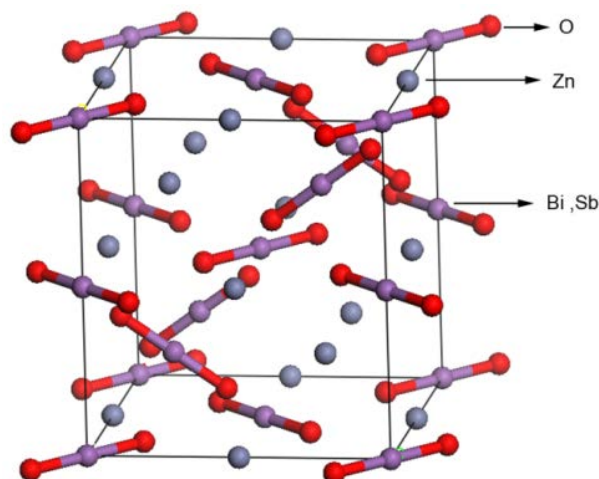


**Table 3.** Structural parameters of  $\text{ZnBiSbO}_4$  calcinated at 800 °C for 35 h.

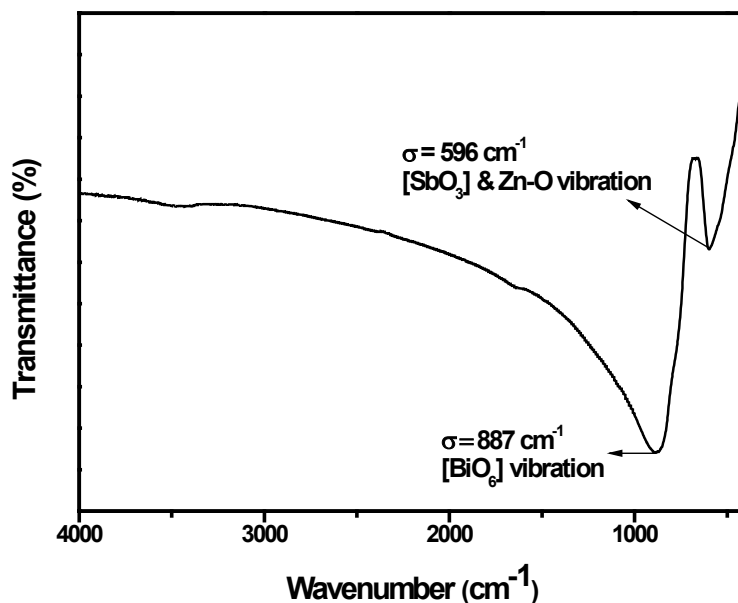
Atom	<i>x</i>	<i>y</i>	<i>z</i>	Occupation factor
Zn	0	0	0.5	1
Bi	0	0	0	1
Sb	0	0	0	1
O	0.76731	0.14013	0.08188	1

**Figure 6.** The structural model of  $\text{ZnBiSbO}_4$  simulated by Materials Studio software corresponding to the XRD pattern shown in Figure 5.



Fourier transform infrared (FTIR) spectrum analysis of ZnBiSbO<sub>4</sub> particles is investigated in this study, as shown in Figure 7. From this picture, we could find that the absorption bands of ZnBiSbO<sub>4</sub> prepared by a solid-state reaction method at 800 °C are at 596 and 887 cm<sup>-1</sup>. The strong band near 887 cm<sup>-1</sup> should be attributed to the Bi–O vibration in the distorted [BiO<sub>6</sub>] unit [47]. The band situated at 596 cm<sup>-1</sup> was overlaid by the symmetric bending and stretching of the [SbO<sub>3</sub>] unit [48] and Zn–O stretching [49].

**Figure 7.** Fourier transform infrared (FTIR) spectrum of ZnBiSbO<sub>4</sub> calcinated at 800 °C for 35 h.



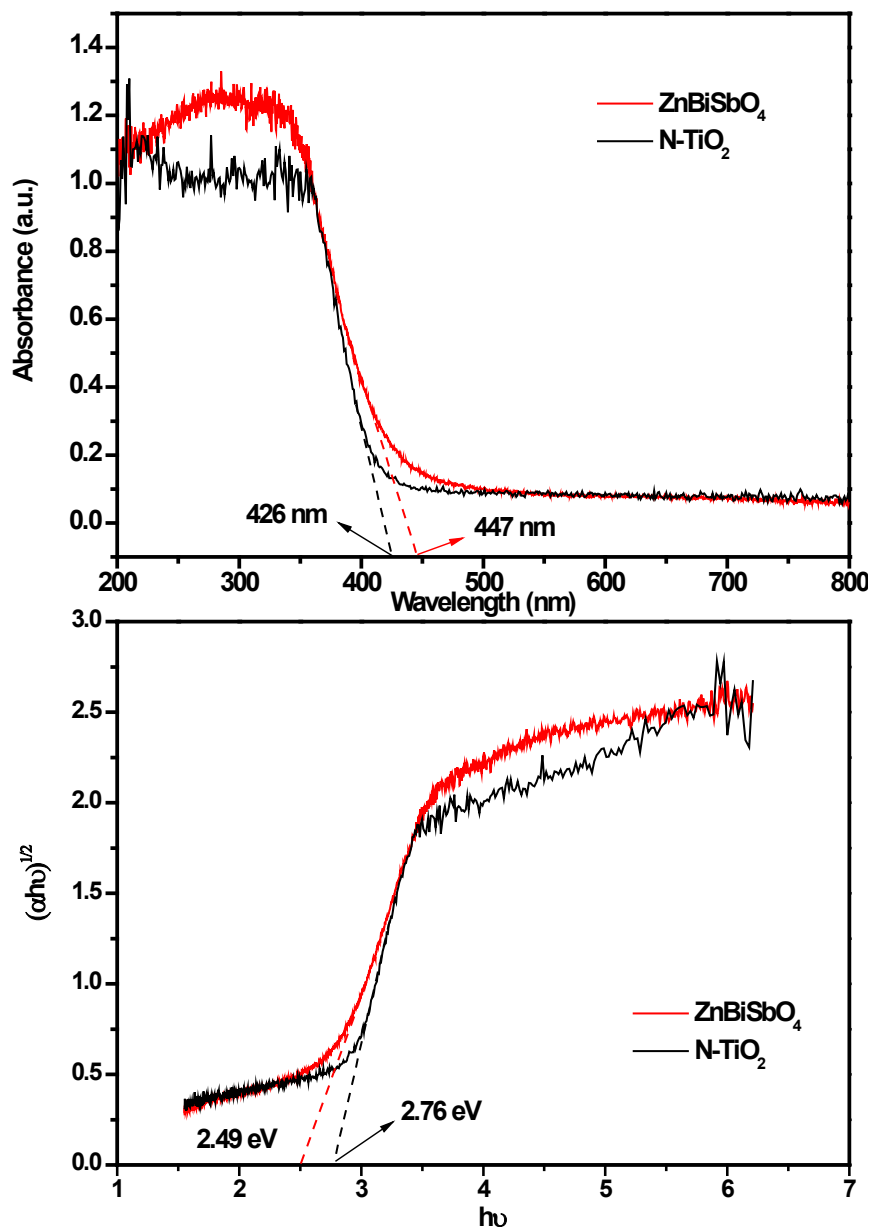
The absorption spectrum of ZnBiSbO<sub>4</sub> is presented in Figure 8. For a crystalline semiconductor, the optical absorption near the band edge following Equation (1) [50]:

$$\alpha h\nu = A \times (h\nu - E_g)^n \quad (1)$$

$$E_g = 1240/\lambda \quad (2)$$

Here,  $A$ ,  $\alpha$ ,  $E_g$ ,  $\nu$  and  $\lambda$  were the proportional constant, absorption coefficient, band gap, light frequency and absorption edge, respectively. In this equation,  $n$  determined the character of the transition in a semiconductor.  $E_g$  and  $n$  could be calculated by the following steps [51]: (i) plotting  $\ln(\alpha h\nu)$  vs.  $\ln(h\nu - E_g)$  by assuming an approximate value of  $E_g$ , which can be calculated by Equation (2); (ii) deducing the value of  $n$ ; and (iii) refining the value of  $E_g$ . From Figure 8, we could find that the absorption edge of ZnBiSbO<sub>4</sub> was about 447 nm, meaning that the estimated  $E_g$  of ZnBiSbO<sub>4</sub> was 2.78 eV. Then, plot  $\ln(\alpha h\nu)$  vs.  $\ln(h\nu - E_g)$ , where we could find the slope of the line part, was about 1.65. Therefore, the  $n$  of ZnBiSbO<sub>4</sub> was two. After plotting  $(\alpha h\nu)^{1/2}$  vs.  $h\nu$  and extrapolating the plot to  $(\alpha h\nu)^{1/2} = 0$ , the accurate value of  $E_g$  of ZnBiSbO<sub>4</sub> was calculated as 2.49 eV. Applying the same calculation process to N-TiO<sub>2</sub>, we found that for N-TiO<sub>2</sub>:  $n = 2$  and  $E_g = 2.76$  eV. The above results indicated that the optical transition for ZnBiSbO<sub>4</sub> or N-TiO<sub>2</sub> was indirectly allowed, and ZnBiSbO<sub>4</sub> possessed a narrow band gap compared with N-TiO<sub>2</sub>. The results in our past work showed that the optical transition for CdBiYO<sub>4</sub> was directly allowed and that the band gap of CdBiYO<sub>4</sub> was 2.41 eV [43].

**Figure 8.** The absorption spectrum, plot of  $(\alpha h\nu)^{1/2}$  vs.  $h\nu$  for ZnBiSbO<sub>4</sub> calcinated at 800 °C for 35 h and N-TiO<sub>2</sub>.



## 2.2. Photocatalytic Properties

The progress of photocatalysis using the semiconductor compound could be described briefly as follows [52,53]. Firstly, the semiconductor compound absorbed photons, resulting in the generation of electron-hole pairs within the semiconductor compound particles and, subsequently, the diffusion of the charge carriers to the surface of the semiconductor compound particle would be followed; at the same time, the active sites of the surface of the semiconductor compound particles had been adsorbing a lot of pollutants particles; finally, the decomposition of pollutants would be performed by charge carriers.

Figure 9 presents the changes in the UV-Vis spectra of IC under visible light irradiation ( $\lambda > 400$  nm) with the presence of ZnBiSbO<sub>4</sub>. The above measurements were performed under oxygen-saturation conditions ( $[\text{O}_2]_{\text{sat}} = 1.02 \times 10^{-3}$  M). It could be clearly noticed from Figure 9 that the typical IC peaks

were at 609.5 nm. An obvious color change from deep red into a colorless solution could be observed within 230 min. For further comparison, Figure 10 depicts the concentration changes of IC with ZnBiSbO<sub>4</sub>, CdBiYO<sub>4</sub> and N-TiO<sub>2</sub> as photocatalysts under visible light irradiation, respectively. It could be seen from Figure 10 that the photonic efficiency ( $\lambda = 420$  nm) was estimated to be 0.0460%, 0.0258% and 0.0304% with ZnBiSbO<sub>4</sub>, N-TiO<sub>2</sub> and CdBiYO<sub>4</sub>, respectively. When ZnBiSbO<sub>4</sub> or CdBiYO<sub>4</sub> or N-TiO<sub>2</sub> was utilized as a catalyst, the photodegradation conversion rate of IC was 98.66% or 65.12% or 55.39% after visible light irradiation for 220 min. The results showed that the photodegradation rate of IC and the photonic efficiency with ZnBiSbO<sub>4</sub> as a catalyst were both higher than those with N-TiO<sub>2</sub> or CdBiYO<sub>4</sub> as a catalyst. The above results showed that complete removal of indigo carmine was observed after visible light irradiation for 230 min with ZnBiSbO<sub>4</sub> as a catalyst. Besides, based on the absorbance changes of IC with irradiation time, the kinetics of IC degradation under visible light irradiation was figured out. The above results demonstrated that the photocatalytic kinetics of IC degradation with ZnBiSbO<sub>4</sub>, CdBiYO<sub>4</sub> and N-TiO<sub>2</sub> as photocatalysts followed a first order nature. The first-order rate constants for IC degradation were estimated to be 0.01945, 0.00405 and 0.00502 min<sup>-1</sup> with ZnBiSbO<sub>4</sub>, N-TiO<sub>2</sub> and CdBiYO<sub>4</sub> as catalysts, respectively. This fact indicated that ZnBiSbO<sub>4</sub> was more efficient than N-TiO<sub>2</sub> or CdBiYO<sub>4</sub> for the photocatalytic degradation of IC under visible light irradiation.

**Figure 9.** Spectral changes of aqueous solutions of indigo carmine (IC) due to visible light irradiation with the presence of ZnBiSbO<sub>4</sub> calcinated at 800 °C for 35 h.

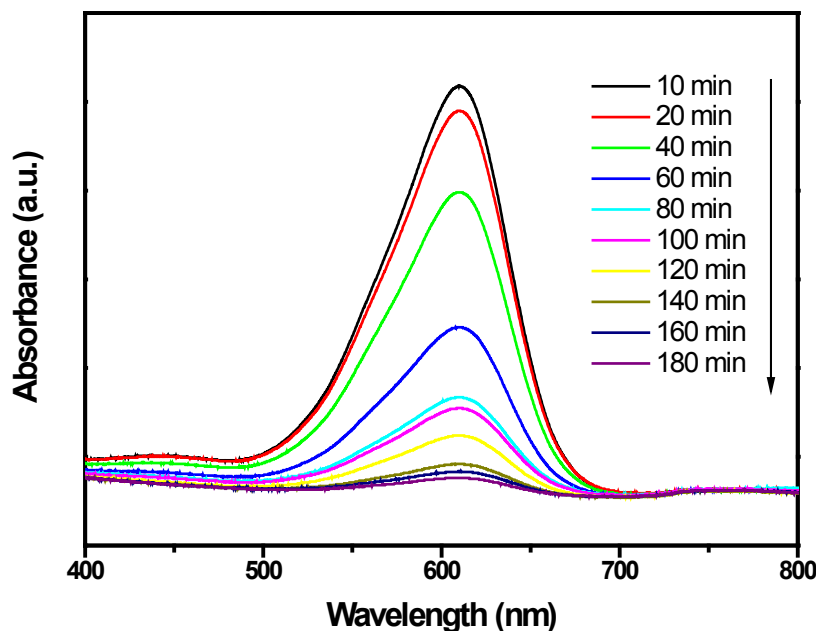


**Figure 10.** Photocatalytic degradation of IC under visible light irradiation with the presence of ZnBiSbO<sub>4</sub>, CdBiYO<sub>4</sub> and N-TiO<sub>2</sub> as photocatalysts, respectively. The results are means of triplicates, and error bars represent  $\pm 1$  SD.

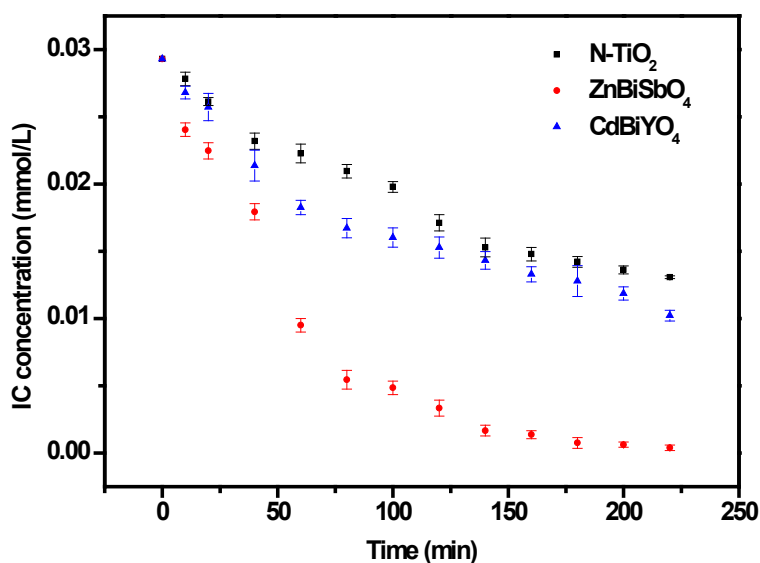
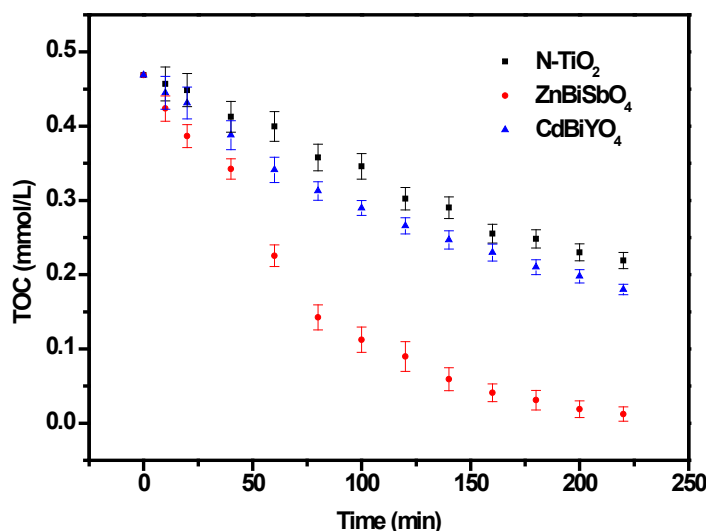


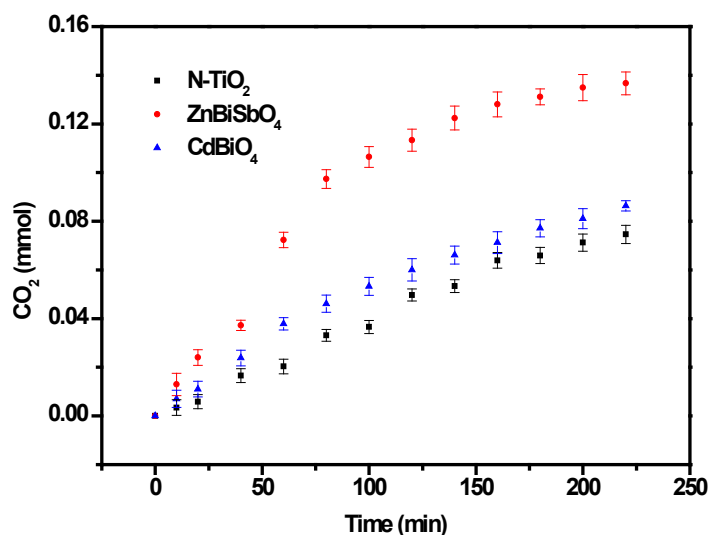
Figure 11 shows the change of total organic carbon (TOC) during the photocatalytic degradation of IC with ZnBiSbO<sub>4</sub>, CdBiYO<sub>4</sub> or N-TiO<sub>2</sub> as a catalyst under visible light irradiation. The TOC measurements revealed the disappearance of organic carbon when the IC solution, which contained ZnBiSbO<sub>4</sub> or CdBiYO<sub>4</sub> or N-TiO<sub>2</sub>, was exposed under visible light irradiation. The results showed that 97.37% or 61.59% or 53.26% of a TOC decrease was obtained after visible light irradiation for 220 min when ZnBiSbO<sub>4</sub> or CdBiYO<sub>4</sub> or N-TiO<sub>2</sub> was utilized as the photocatalyst. Consequently, it could be seen from Figure 11 that the entire mineralization of indigo carmine was realized after visible light irradiation for 270 min with ZnBiSbO<sub>4</sub> as a catalyst, because of the 100% TOC removal. The apparent first order rate constant,  $k$ , was estimated to be 0.01536, 0.00449 and 0.00350 min<sup>-1</sup> with ZnBiSbO<sub>4</sub>, CdBiYO<sub>4</sub> or N-TiO<sub>2</sub> as the photocatalyst, respectively.

During the progress of IC degradation, IC was converted into smaller organic species and was ultimately mineralized to inorganic products, such as carbon dioxide and water. Figure 12 presents the CO<sub>2</sub> yield during the photocatalytic degradation of IC with ZnBiSbO<sub>4</sub> or CdBiYO<sub>4</sub> or N-TiO<sub>2</sub> as the photocatalyst under visible light irradiation. The amount of CO<sub>2</sub> increased gradually with increasing reaction time when IC was photodegraded with ZnBiSbO<sub>4</sub> or CdBiYO<sub>4</sub> or N-TiO<sub>2</sub> as the photocatalyst. The results showed that the production rate of CO<sub>2</sub> from the ZnBiSbO<sub>4</sub>-IC system was higher than that from the CdBiYO<sub>4</sub>-IC system or N-TiO<sub>2</sub>-IC system with increasing reaction time. For example, the production amount of CO<sub>2</sub> was 0.08103 or 0.07122 mmol with CdBiYO<sub>4</sub> or N-TiO<sub>2</sub> as the photocatalyst after a visible light irradiation of 200 min. However, the production amount of CO<sub>2</sub> was 0.1349 mmol with ZnBiSbO<sub>4</sub> as the photocatalyst after a visible light irradiation of 200 min.

**Figure 11.** Total organic carbon (TOC) plots during the photocatalytic degradation of IC under visible light irradiation with  $\text{ZnBiSbO}_4$ ,  $\text{CdBiYO}_4$  and  $\text{N-TiO}_2$  as photocatalysts, respectively. The results are means of triplicates, and error bars represent  $\pm 1$  SD.



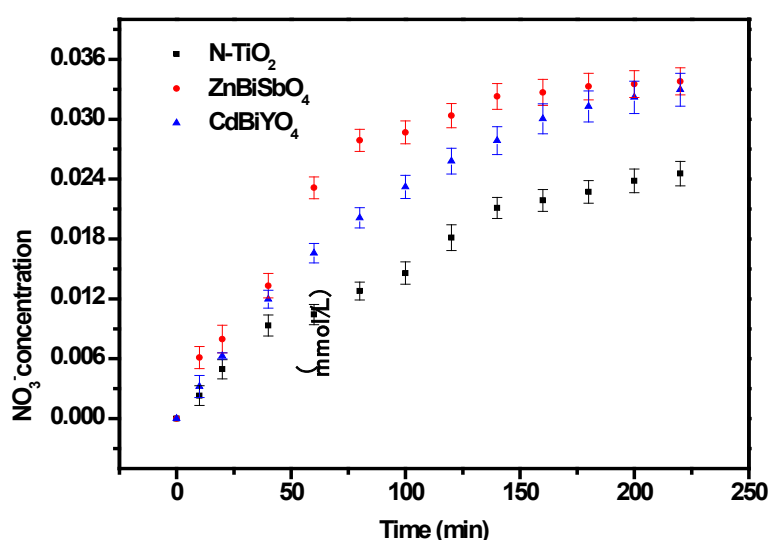
**Figure 12.**  $\text{CO}_2$  production during the photocatalytic degradation of IC with  $\text{ZnBiSbO}_4$ ,  $\text{CdBiYO}_4$  and  $\text{N-TiO}_2$  as photocatalysts, respectively, under visible light irradiation. The results are means of triplicates, and error bars represent  $\pm 1$  SD.



In order to explore the mechanism of the IC degradation with  $\text{ZnBiSbO}_4$  or  $\text{CdBiYO}_4$  or  $\text{N-TiO}_2$  as photocatalyst under visible light irradiation, we also tested the concentration of inorganic ions,  $\text{NO}_3^-$  and  $\text{SO}_4^{2-}$ , which are shown in Figures 13 and 14, which may be formed as the end products of nitrogen and sulfur atoms that existed in IC. From Figures 13 and 14, we could be sure that both  $\text{NO}_3^-$  and  $\text{SO}_4^{2-}$  appeared during IC degradation with  $\text{ZnBiSbO}_4$  or  $\text{CdBiYO}_4$  or  $\text{N-TiO}_2$  as the photocatalyst.  $\text{NO}_3^-$  and  $\text{SO}_4^{2-}$  ions were generated more quickly and effectively with  $\text{ZnBiSbO}_4$  compared with  $\text{N-TiO}_2$  or  $\text{CdBiYO}_4$  as photocatalyst, which was in accord with the above analysis about the degradation progress of IC. According to the  $\text{NO}_3^-$  concentration in Figure 13, we could calculate that 57.66% or 68.95% or 41.89% of sulfur from IC was converted into sulfate ions with  $\text{ZnBiSbO}_4$  or  $\text{CdBiYO}_4$  or  $\text{N-TiO}_2$  as the photocatalyst after visible light irradiation for 220 min. Meanwhile, it could

be also concluded that 64.32% or 60.09% or 39.11% of sulfur from IC was converted into sulfate ions with ZnBiSbO<sub>4</sub> or CdBiYO<sub>4</sub> or N-TiO<sub>2</sub> as photocatalyst after visible light irradiation for 220 min. It was noteworthy that the amount of SO<sub>4</sub><sup>2-</sup> and NO<sub>3</sub><sup>-</sup> that were released into the solution were sharply lower than the stoichiometry value of 100%. One possible reason could be a loss of sulfur-containing volatile compounds or SO<sub>2</sub> for the S element and nitrogen-containing volatile compounds or NH<sub>3</sub>. The second possible reason was a partially irreversible adsorption of some SO<sub>4</sub><sup>2-</sup> and NO<sub>3</sub><sup>-</sup> on the surface of the photocatalyst, which had been observed by Lachheb *et al.* with titanium dioxide [54].

**Figure 13.** NO<sub>3</sub><sup>-</sup> production during the photocatalytic degradation of IC with ZnBiSbO<sub>4</sub>, CdBiYO<sub>4</sub> and N-TiO<sub>2</sub> as photocatalysts, respectively, under visible light irradiation. The results are means of triplicates, and error bars represent ±1 SD.



In addition, the intermediates generated during the degradation process were detected by high-performance liquid chromatography (HPLC) and gas chromatography-mass spectrometry (GC-MS) and identified by comparison with commercial standard samples. The intermediates in our experiment were identified as follows: indoline-2,3-dione, anthranilic acid, *O*-nitrobenzyl dehyde, aniline, ethene-1,2-diol, amino-fumaric acid, oxalic acid, glycolal dehyde and acetic acid. The sulfur was first hydrolytically removed and subsequently was oxidized and transformed into SO<sub>4</sub><sup>2-</sup>. At the same time, nitrogen atoms in the -3 oxidation state produced NH<sub>4</sub><sup>+</sup> cations that subsequently were oxidized into NO<sub>3</sub><sup>-</sup> ions. Based on the above results, we have deduced a degradation pathway of IC with ZnBiSbO<sub>4</sub>, as shown in Figure 15. This pathway was similar, but not identical, to the pathway proposed by Manon Vautier *et al.* [55]. According to Figure 15, the main degradation end-products of IC were CO<sub>2</sub>, NO<sub>3</sub><sup>-</sup> and SO<sub>4</sub><sup>2-</sup>. Thus, the mass balance of the C, N and S elements from IC (reaction time = 0 min) to end-products (reaction time = 220 min) during the degradation process of IC in the reactor had been studied. The original amount of C within IC was 140.64 μmol, which was close to the amount of C within the end-product, CO<sub>2</sub> (137.00 μmol). The value of the original amount of N within IC vs. the one within end-product NO<sub>3</sub><sup>-</sup> was 17.58 μmol/10.20 μmol. The value of the original amount of N within IC vs. the one within end-product NO<sub>3</sub><sup>-</sup> was 17.58 μmol/11.40 μmol. The above results agreed with the analysis about Figures 12–14.

**Figure 14.**  $\text{SO}_4^{2-}$  production during the photocatalytic degradation of IC with  $\text{ZnBiSbO}_4$ ,  $\text{CdBiYO}_4$  and  $\text{N-TiO}_2$  as photocatalysts, respectively, under visible light irradiation. The results are the means of triplicates, and error bars represent  $\pm 1$  SD.

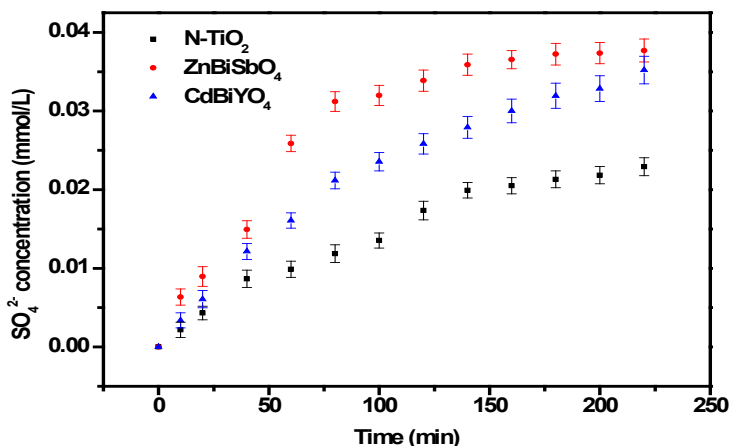
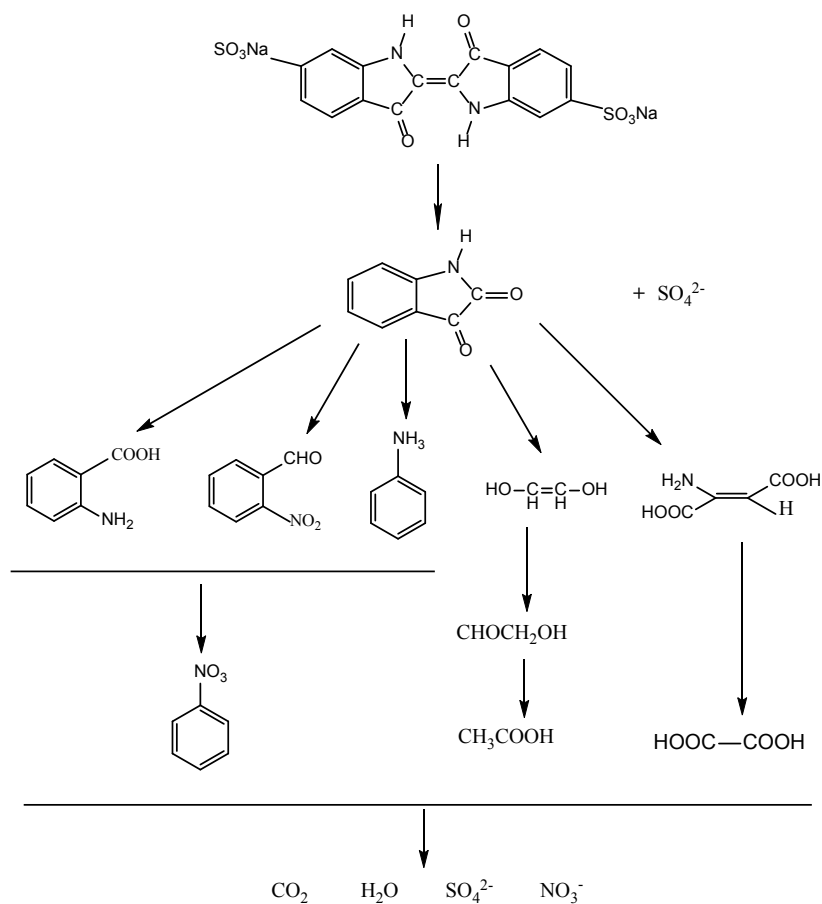


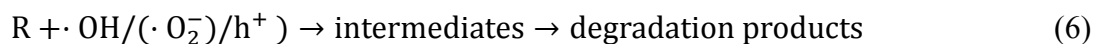
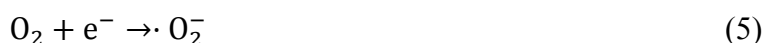
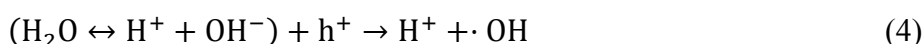
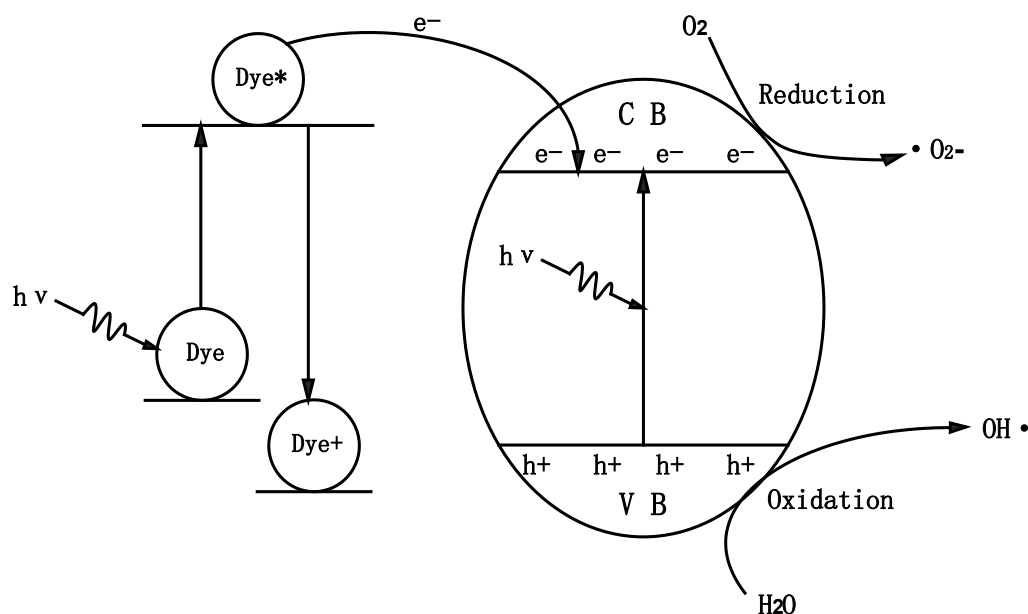
**Figure 15.** Suggested photocatalytic degradation pathway scheme for IC under visible light irradiation with the presence of  $\text{ZnBiSbO}_4$  prepared by a solid-state reaction method at  $800\text{ }^\circ\text{C}$  for 35 h.



A mechanism scheme of the charge separation and photocatalytic reaction for  $\text{ZnBiSbO}_4$  is shown in Figure 16. Firstly, photoinduced holes ( $\text{h}^+$ ) and photoinduced electrons ( $\text{e}^-$ ) came into being in the surface of  $\text{ZnBiSbO}_4$  particles (Equation (3)). Secondly, organic pollutants (R) could be degraded into

inorganic products with the effluence of  $h^+$  and  $e^-$ . Many published works [56–58] had confirmed that two oxidative agents could be mainly concerned under visible light irradiation:  $\text{OH}\cdot$ -radicals and  $\cdot\text{O}_2^-$  radicals. Then,  $h^+$  reacted with R directly (Equations (4)–(6)). Besides, the effect of dye sensitization should be taken into consideration (Equations (7) and (8)); because IC could be excited by visible light, and then, the sensitizing dye molecules injected electrons into the semiconductor nanocrystallites, which were collected at a conducting surface to generate the photocurrent (Equation (9)) [59,60].

**Figure 16.** Suggested photodegradation reaction mechanism of IC with  $\text{ZnBiSbO}_4$  as the photocatalyst under visible light irradiation. (CB, Conduction Band; VB, Valence Band)



### 2.3. Phytotoxicity Properties

The phytotoxicity of the photocatalytic-treated IC wastewater was detected by examining its effect on seed germination and growth as shown in Tables 4 and 5. We could find that when indigo carmine wastewater was straightly used for agriculture, it was so hazardous to the environment that the seeds could not survive. It could be seen from Tables 4 and 5 that germinations, the lengths of the plumule and radicle of *Triticum aestivum* and *Sorghum vulgare* seeds went up consistently with increasing the photocatalytic reaction time. The above result revealed that the metabolites generated during the photodegradation of IC wastewater were less toxic than the compound in the original IC wastewater.

Moreover, the growth conditions of the seeds cultured by IC wastewater after 220 min of photocatalytic reaction were approximate to the control group. The phytotoxicity experiment results demonstrated that the photocatalytic degradation with  $\text{ZnBiSbO}_4$  as a catalyst under visible light irradiation had a significant positive effect on IC wastewater treatment.

**Table 4.** The phytotoxicity study for *Sorghum vulgare* seeds by using treated IC wastewater. The results are the mean of triplicates (mean  $\pm$  SD).

Parameters	<i>Sorghum vulgare</i>						
	Control	Sample of different photocatalytic reaction time (min)					
		0	40	80	120	160	220
Germination (%)	100	0	7.2 $\pm$ 0.6	21 $\pm$ 4.1	44 $\pm$ 6.5	68 $\pm$ 8.0	92 $\pm$ 3.5
Plumule (cm)	9.82 $\pm$ 1.23	0	1.15 $\pm$ 0.18	2.02 $\pm$ 0.36	4.16 $\pm$ 0.58	5.33 $\pm$ 0.79	8.54 $\pm$ 1.23
Radicle (cm)	6.79 $\pm$ 9.52	0	0.36 $\pm$ 0.12	1.04 $\pm$ 0.22	2.29 $\pm$ 0.29	3.22 $\pm$ 0.54	5.47 $\pm$ 0.89

**Table 5.** The phytotoxicity study for *Triticum aestivum* seeds by using treated IC wastewater. The results are the mean of triplicates (mean  $\pm$  SD).

Parameters	<i>Triticum aestivum</i>						
	Control	Sample of different photocatalytic reaction time (min)					
		0	40	80	120	160	220
Germination (%)	100	0	5.7 $\pm$ 1.3	16 $\pm$ 2.0	37 $\pm$ 6.4	63 $\pm$ 8.7	87 $\pm$ 2.5
Plumule (cm)	8.24 $\pm$ 1.12	0	1.02 $\pm$ 0.22	1.79 $\pm$ 0.29	3.84 $\pm$ 0.68	5.11 $\pm$ 0.82	8.32 $\pm$ 1.25
Radicle (cm)	6.13 $\pm$ 1.07	0	0.31 $\pm$ 0.05	0.96 $\pm$ 0.14	2.03 $\pm$ 0.57	3.02 $\pm$ 0.44	5.25 $\pm$ 0.78

### 3. Experimental Section

#### 3.1. Synthesis of Nanocatalyst

The novel photocatalysts,  $\text{ZnBiSbO}_4$  and  $\text{CdBiYO}_4$ , were prepared by the solid-state reaction method.  $\text{ZnO}$ ,  $\text{Bi}_2\text{O}_3$  and  $\text{Sb}_2\text{O}_3$  with a purity of 99.99% (Sinopharm Group Chemical Reagent Co., Ltd., Shanghai, China) were used as raw materials. In order to synthesize  $\text{ZnBiSbO}_4$ , the precursors were stoichiometrically mixed in a quartz mortar, then pressed into small columns and put into an alumina crucible (Shenyang Crucible Co., Ltd., Shenyang, China). Finally, calcination was carried out at 800 °C for 35 h in an electric furnace (KSL 1700X, Hefei Kejing Materials Technology Co., Ltd., Hefei, China). The last step was sintering and grinding with a quartz mortar, and then,  $\text{ZnBiSbO}_4$  powder was fabricated.  $\text{CdO}$ ,  $\text{Bi}_2\text{O}_3$  and  $\text{Y}_2\text{O}_3$  with a purity of 99.99% were utilized as raw materials and utilized without further purification. All powders were dried at 200 °C for 4 h before synthesis. In order to synthesize  $\text{CdBiYO}_4$ , the precursors were stoichiometrically mixed in a quartz mortar, subsequently pressed into small columns and put into an alumina crucible. Finally, calcination was carried out at 900 °C for 36 h in an electric furnace. Nitrogen-doped titania ( $\text{N-TiO}_2$ ) catalyst with tetrabutyl titanate as a titanium precursor was prepared by using the sol-gel method at room temperature. The following procedure was that 17 mL tetrabutyl titanate and 40 mL absolute ethyl alcohol were mixed as Solution A; subsequently, Solution A was added dropwise under vigorous stirring into the Solution B that contained 40 mL absolute ethyl alcohol, 10 mL glacial acetic acid and

5 mL double distilled water to form transparent colloidal Suspension C. Subsequently, aqua ammonia with N/Ti proportion of 8 mol % was added into the resulting transparent colloidal suspension under vigorous stirring condition and stirred for 1 h. Finally, the xerogel was formed after being aged for 2 days. The xerogel was ground into powder, which was calcinated at 500 °C for 2 h; subsequently, the above powder was ground in an agate mortar and screened by a shaker to obtain N-TiO<sub>2</sub> powders.

### 3.2. Characterization of ZnBiSbO<sub>4</sub>

The particle morphologies of ZnBiSbO<sub>4</sub> were measured by transmission electron microscope (TEM, Tecna F20 S-Twin, FEI Corporation, Hillsboro, OR, USA). The chemical composition of the compound was determined by a scanning electron microscope, which was equipped with X-ray energy dispersion spectrum (SEM-EDS, LEO 1530VP, LEO Corporation, Peggitz, Germany) and X-ray photoelectron spectroscopy (XPS, ESCALABMK-2, VG Scientific Ltd., East Grinstead, UK). The Zn<sup>2+</sup> content, Bi<sup>3+</sup> content, Sb<sup>3+</sup> content and O<sup>2-</sup> content of ZnBiSbO<sub>4</sub> and the valence state of the elements were also analyzed by X-ray photoelectron spectroscopy. The chemical composition within the depth profile of ZnBiSbO<sub>4</sub> was examined by the argon ion denudation method when X-ray photoelectron spectroscopy was utilized. The particle sizes of ZnBiSbO<sub>4</sub> were measured by Malvern's mastersize-2000 particle size analyzer (Malvern Instruments Ltd., Malvern, UK). The crystalline phase of ZnBiSbO<sub>4</sub> was analyzed by X-ray diffractometer (D/MAX-RB, Rigaku Corporation, Tokyo, Japan) with Cu-K $\alpha$  radiation ( $\lambda = 1.54056 \text{ \AA}$ ). The patterns were collected at 295 K with a step-scan procedure in the range of  $2\theta = 10^\circ\text{--}100^\circ$ . The step interval was  $0.02^\circ$ , and the time per step was 1 s. The accelerating voltage and applied current were 40 kV and 40 mA, respectively. Fourier transform infrared spectroscopy (FTIR, Nexus, Nicolet Corporation, Madison, WI, USA) was used to examine the FTIR spectra of ZnBiSbO<sub>4</sub>. The UV-visible diffuse reflectance spectrum of ZnBiSbO<sub>4</sub> was measured with a Shimadzu UV-2550 UV-Visible spectrometer (Shimadzu, Santa Clara, CA, USA), and BaSO<sub>4</sub> was utilized as the reference material. The Brunauer–Emmett–Teller (BET) surface area was detected by nitrogen-sorption using a Micromeritics ASAP 2020 analyzer (Micromeritics, Atlanta, GA, USA).

### 3.3. Photocatalytic Activity Experiments

The photocatalytic activity of ZnBiSbO<sub>4</sub> was evaluated with indigo carmine (IC) (C<sub>16</sub>H<sub>8</sub>N<sub>2</sub>Na<sub>2</sub>O<sub>8</sub>S<sub>2</sub>) (Tianjin Bodi Chemical Co., Ltd., Tianjin, China) as the model material. The photoreaction was carried out in a photochemical reaction apparatus (Nanjing Xujiang Machine Plant, Nanjing, China). The internal structure of the reaction apparatus was as following: the lamp was put into a quartz hydrazine, which was a hollow structure, and located in the middle of the reactor. The recycling water through the reactor maintained at a near constant reaction temperature (20 °C), and the solution was continuously stirred and aerated. Twelve holes were utilized to put quartz tubes evenly distributed around the lamp, and the distance between the lamp and each hole was equal. Under the condition of magnetic stirring, the photocatalyst within the IC solution was in a state of suspension. In this paper, the photocatalytic degradation of IC was performed with 0.3 g ZnBiSbO<sub>4</sub> in a 300-mL, 29.3- $\mu\text{mol/L}$  IC aqueous solution in quartz tubes with 500 W Xenon lamp ( $400 \text{ nm} < \lambda < 800 \text{ nm}$ ) as the visible light source. Prior to visible light irradiation, the suspensions, which contained the catalyst and IC dye,

were magnetically stirred in darkness for 45 min to ensure the establishment of an adsorption/desorption equilibrium among  $\text{ZnBiSbO}_4$ , the IC dye and atmospheric oxygen. During visible light illumination, the suspension was stirred at 500 rpm, and the initial pH value of the IC solution was 7.0 without pH value adjustment in the reaction process. The above experiments were performed under oxygen-saturation conditions ( $[\text{O}_2]_{\text{sat}} = 1.02 \times 10^{-3} \text{ mol/L}$ ). One of the quartz tubes was taken out from the photochemical reaction apparatus at various time intervals. The suspension was filtered through 0.22- $\mu\text{m}$  membrane filters. The filtrate was subsequently analyzed by a Shimadzu UV-2450 spectrometer (Shimadzu, Santa Clara, CA, USA) with a detecting wavelength at 610 nm. The experimental error was found to be within  $\pm 2.2\%$ .

The photonic efficiency was calculated according to the following Equation (10) [61,62]:

$$\xi = R/I_0 \quad (10)$$

where  $\xi$  was the photonic efficiency (%),  $R$  was the rate of indigo carmine degradation ( $\text{mol}\cdot\text{L}^{-1}\cdot\text{s}^{-1}$ ), which indicated the concentration decrement of indigo carmine within every second, and  $I_0$  was the incident photon flux ( $\text{Einstein}\cdot\text{L}^{-1}\cdot\text{s}^{-1}$ ). The incident photon flux,  $I_0$ , which was measured by a radiometer (Model FZ-A, Photoelectric Instrument Factory, Beijing Normal University, Beijing, China), was determined to be  $4.76 \times 10^{-6} \text{ Einstein}\cdot\text{L}^{-1}\cdot\text{s}^{-1}$  under visible light irradiation (a wavelength range of 400–700 nm).

#### 3.4. Phytotoxicity Experiments

The phytotoxicity study was carried out by using *Triticum aestivum* and *Sorghum vulgare* seeds. Fifteen seeds of *Triticum aestivum* or *Sorghum vulgare* were placed over two sheets of filter paper (Whatman No. 42) in  $110 \times 20 \text{ mm}$  glass petri dishes at room temperature. Subsequently, IC effluent samples (15 mL) were added to each petri dish, respectively. Control groups contained 15 mL distilled water, instead of effluents, at the same time. Germination (%) and the length of the plumule and radicle were recorded after 9 days.

#### 4. Conclusions

In summary, newly synthesized photocatalyst  $\text{ZnBiSbO}_4$  showed higher photocatalytic activity compared with  $\text{N-TiO}_2$  or  $\text{CdBiYO}_4$  for the photocatalytic degradation of indigo carmine under visible light irradiation. The photocatalytic degradation of indigo carmine with  $\text{ZnBiSbO}_4$  as a catalyst followed the first-order reaction kinetics. The possible photocatalytic degradation pathway of indigo carmine was obtained. The phytotoxicity of the photocatalytic-treated IC wastewater was detected by examining its effect on seed germination and growth. The phytotoxicity experiment results demonstrated that the photocatalytic degradation with  $\text{ZnBiSbO}_4$  as a catalyst under visible light irradiation had a significant positive effect on IC wastewater treatment. The results obtained in our investigations proved that  $\text{ZnBiSbO}_4/(\text{visible light})$  photocatalysis might be regarded as a method for the practical treatment of diluted colored waste water in the environment of room-temperature and ordinary pressure.

## Acknowledgments

This work was supported by the National Natural Science Foundation of China (No. 21277067). This work was supported by a grant from the China-Israel Joint Research Program in Water Technology and Renewable Energy (No. 5). This work was supported by a grant from The Fourth Technological Development Scheming (Industry) Program of Suzhou City of China from 2010 (SYG201006). This work was supported by a grant from the Fundamental Research Funds for the Central Universities.

## Author Contributions

Jingfei Luan and Mengjing Chen conceived and designed the experiment project. Mengjing Chen, Jingfei Luan and Wenhua Hu performed the experiments. Jingfei Luan and Mengjing Chen wrote the paper. All authors read and approved the manuscript.

## Conflicts of Interest

The authors declare no conflict of interest.

## References

1. Siddique, M.; Farooq, R.; Khalid, A.; Farooq, A.; Mahmood, Q.; Farooq, U.; Raja, I.A.; Shaukat, S.F. Thermal-pressure-mediated hydrolysis of reactive blue 19 dye. *J. Hazard. Mater.* **2009**, *172*, 1007–1012.
2. Wang, S.B.; Li, H.T. Dye adsorption on unburned carbon: Kinetics and equilibrium. *J. Hazard. Mater.* **2005**, *126*, 71–77.
3. Zhang, M.Y.; Shao, C.L.; Guo, Z.C.; Zhang, Z.Y.; Mu, J.B.; Zhang, P.; Cao, T.P.; Liu, Y.C. Highly efficient decomposition of organic dye by aqueous-solid phase transfer and *in situ* photocatalysis using hierarchical copper phthalocyanine hollow spheres. *ACS Appl. Mater. Interfaces* **2011**, *3*, 2573–2578.
4. Hoffmann, M.R.; Martin, S.T.; Choi, W.Y.; Bahnemann, D.W. Environmental applications of semiconductor photocatalysis. *Chem. Rev.* **1995**, *95*, 69–96.
5. Binding, D.; Steinbach, F. Homogeneous photocatalysis by organic dyes in liquid phase. *Nature* **1970**, *227*, 832–833.
6. Luan, J.F.; Pan, B.C.; Paz, Y.; Li, Y.M.; Wu, X.S.; Zou, Z.G. Structural, photophysical and photocatalytic properties of new Bi<sub>2</sub>SbVO<sub>7</sub> under visible light irradiation. *Phys. Chem. Chem. Phys.* **2009**, *11*, 6289–6298.
7. Wang, C.; Zhao, J.C.; Wang, X.M.; Mai, B.X.; Sheng, G.Y.; Peng, P.; Fu, J.M. Preparation, characterization and photocatalytic activity of nano-sized ZnO/SnO<sub>2</sub> coupled photocatalysts. *Appl. Catal. B* **2002**, *39*, 269–279.
8. Zhang, L.; Zhang, J.P.; Wu, Z.N. Pesticide removal from water suspension by UV/TiO<sub>2</sub> process: A parametric study. *Desalin. Water Treat.* **2014**, *52*, 1956–1964.
9. Linsebigler, A.L.; Lu, G.Q.; Yates, J.T. Photocatalysis on TiO<sub>2</sub> surfaces—Principles, mechanisms, and selected results. *Chem. Rev.* **1995**, *95*, 735–758.

10. Torimoto, T.; Ito, S.; Kuwabata, S.; Yoneyama, H. Effects of adsorbents used as supports for titanium dioxide loading on photocatalytic degradation of propyzamide. *Environ. Sci. Technol.* **1996**, *30*, 1275–1281.
11. Pham, T.D.; Lee, B.K. Cu doped TiO<sub>2</sub>/GF for photocatalytic disinfection of escherichia coli in bioaerosols under visible light irradiation: Application and mechanism. *Appl. Surf. Sci.* **2014**, *296*, 15–23.
12. Shirsath, S.R.; Pinjari, D.V.; Gogate, P.R.; Sonawane, S.H.; Pandit, A.B. Ultrasound assisted synthesis of doped TiO<sub>2</sub> nano-particles: Characterization and comparison of effectiveness for photocatalytic oxidation of dyestuff effluent. *Ultrason. Sonochem.* **2013**, *20*, 277–286.
13. Charanpahari, A.; Umare, S.S.; Gokhale, S.P.; Sudarsan, V.; Sreedhar, B.; Sasikala, R. Enhanced photocatalytic activity of multi-doped TiO<sub>2</sub> for the degradation of methyl orange. *Appl. Catal. A* **2012**, *443*, 96–102.
14. Karunakaran, C.; SakthiRaadha, S.; Gomathisankar, P. Hot-injection synthesis of bactericidal Sn-doped TiO<sub>2</sub> nanospheres for visible-light photocatalysis. *Mater. Express* **2012**, *2*, 319–326.
15. Sano, T.; Mera, N.; Kanai, Y.; Nishimoto, C.; Tsutsui, S.; Hiramawa, T.; Negishi, N. Origin of visible-light activity of *n*-doped TiO<sub>2</sub> photocatalyst: Behaviors of N and S atoms in a wet *n*-doping process. *Appl. Catal. B* **2012**, *128*, 77–83.
16. Neville, E.M.; Mattle, M.J.; Loughrey, D.; Rajesh, B.; Rahman, M.; MacElroy, J.M.D.; Sullivan, J.A.; Thampi, K.R. Carbon-doped TiO<sub>2</sub> and carbon, tungsten-codoped TiO<sub>2</sub> through sol-gel processes in the presence of melamine borate: Reflections through photocatalysis. *J. Phys. Chem. C* **2012**, *116*, 16511–16521.
17. Wang, W.; Lu, C.H.; Ni, Y.R.; Su, M.X.; Xu, Z.Z. A new sight on hydrogenation of F and N–F doped {001} facets dominated anatase TiO<sub>2</sub> for efficient visible light photocatalyst. *Appl. Catal. B* **2012**, *127*, 28–35.
18. Ma, X.G.; Wu, Y.; Lu, Y.H.; Xu, J.; Wang, Y.J.; Zhu, Y.F. Effect of compensated codoping on the photoelectrochemical properties of anatase TiO<sub>2</sub> photocatalyst. *J. Phys. Chem. C* **2011**, *115*, 16963–16969.
19. Zhang, M.L.; Li, L.F.; Meng, X.D. A simple new way to prepare Cu-doped nano-TiO<sub>2</sub> with visible light photocatalytic activity. *Adv. Mater. Res.* **2011**, *197–198*, 1028–1031.
20. Ochiai, T.; Fujishima, A. Photoelectrochemical properties of TiO<sub>2</sub> photocatalyst and its applications for environmental purification. *J. Photochem. Photobiol. C* **2012**, *13*, 247–262.
21. Rawal, S.B.; Bera, S.; Lee, W.I. Visible-light photocatalytic properties of W<sub>18</sub>O<sub>19</sub>/TiO<sub>2</sub> and WO<sub>3</sub>/TiO<sub>2</sub> heterocomposites. *Catal. Lett.* **2012**, *142*, 1482–1488.
22. Su, K.; Ai, Z.H.; Zhang, L.Z. Efficient visible light-driven photocatalytic degradation of pentachlorophenol with Bi<sub>2</sub>O<sub>3</sub>/TiO<sub>2</sub>-*x*B<sub>x</sub>. *J. Phys. Chem. C* **2012**, *116*, 17118–17123.
23. Wu, D.W.; Li, S.; Zhang, Q.L.; Chen, Y.Q.; Gong, M.C. Composite photocatalyst TiO<sub>2</sub>/BiNbO<sub>4</sub>: Preparation and degradation performance for gas phase benzene. *Chin. J. Inorg. Chem.* **2012**, *28*, 1383–1388.
24. Fei, X.N.; Jia, G.Z.; Xu, X.J.; Hao, Y.C.; Wang, D.; Guo, J. Study on preparation and sunlight photocatalytic activity of porous coupled ZnO/TiO<sub>2</sub> photocatalyst. *Optoelectron. Adv. Mater.* **2012**, *6*, 709–712.

25. Lin, B.Z.; Li, X.L.; Xu, B.H.; Chen, Y.L.; Gao, B.F.; Fan, X.R. Improved photocatalytic activity of anatase TiO<sub>2</sub>-pillared HTaWO<sub>6</sub> for degradation of methylene blue. *Microporous Mesoporous Mater.* **2012**, *155*, 16–23.
26. Chai, B.; Peng, T.Y.; Mao, J.; Li, K.; Zan, L. Graphitic carbon nitride (g-C<sub>3</sub>N<sub>4</sub>)-Pt-TiO<sub>2</sub> nanocomposite as an efficient photocatalyst for hydrogen production under visible light irradiation. *Phys. Chem. Chem. Phys.* **2012**, *14*, 16745–16752.
27. Sun, M.; Chen, G.D.; Zhang, Y.K.; Wei, Q.; Ma, Z.M.; Du, B. Efficient degradation of azo dyes over Sb<sub>2</sub>S<sub>3</sub>/TiO<sub>2</sub> heterojunction under visible light irradiation. *Ind. Eng. Chem. Res.* **2012**, *51*, 2897–2903.
28. Qian, S.S.; Wang, C.S.; Liu, W.J.; Zhu, Y.H.; Yao, W.J.; Lu, X.H. An enhanced CdS/TiO<sub>2</sub> photocatalyst with high stability and activity: Effect of mesoporous substrate and bifunctional linking molecule. *J. Mater. Chem.* **2011**, *21*, 4945–4952.
29. Cropek, D.; Kemme, P.A.; Makarova, O.V.; Chen, L.X.; Rajh, T. Selective photocatalytic decomposition of nitrobenzene using surface modified TiO<sub>2</sub> nanoparticles. *J. Phys. Chem. C* **2008**, *112*, 8311–8318.
30. Lu, W.S.; Xiao, G.C.; Li, D.Z.; Fu, X.Z.; Wang, X.X. Synthesis and characterization of visible light-driven photocatalyst Pt/InVO<sub>4</sub>/TiO<sub>2</sub>. *Chin. J. Inorg. Chem.* **2005**, *21*, 1495–1499.
31. Tatsuma, T.; Saitoh, S.; Ngaotrakanwivat, P.; Ohko, Y.; Fujishima, A. Energy storage of TiO<sub>2</sub>-WO<sub>3</sub> photocatalysis systems in the gas phase. *Langmuir* **2002**, *18*, 7777–7779.
32. Zhang, X.; Ai, Z.H.; Jia, F.L.; Zhang, L.Z.; Fan, X.X.; Zou, Z.G. Selective synthesis and visible-light photocatalytic activities of BiVO<sub>4</sub> with different crystalline phases. *Mater. Chem. Phys.* **2007**, *103*, 162–167.
33. Zhou, J.K.; Zou, Z.G.; Ray, A.K.; Zhao, X.S. Preparation and characterization of polycrystalline bismuth titanate Bi<sub>12</sub>TiO<sub>20</sub> and its photocatalytic properties under visible light irradiation. *Ind. Eng. Chem. Res.* **2007**, *46*, 745–749.
34. Zhang, G.K.; Zou, X.; Gong, J.; He, F.S.; Zhang, H.; Zhang, Q.; Liu, Y.; Yang, X.; Hu, B. Preparation and photocatalytic property of potassium niobate K<sub>6</sub>Nb<sub>10.8</sub>O<sub>30</sub>. *J. Alloy. Compd.* **2006**, *425*, 76–80.
35. Peng, F.; Zhou, C.M.; Wang, H.J.; Yu, H.; Liang, J.H.; Yang, J.A. The role of RuO<sub>2</sub> in the electrocatalytic oxidation of methanol for direct methanol fuel cell. *Catal. Commun.* **2009**, *10*, 533–537.
36. Li, X.K.; Kako, T.; Ye, J.H. 2-Propanol photodegradation over lead niobates under visible light irradiation. *Appl. Catal. A* **2007**, *326*, 1–7.
37. Hou, L.R.; Yuan, C.Z.; Peng, Y. Preparation and photocatalytic property of sunlight-driven photocatalyst Bi<sub>38</sub>ZnO<sub>58</sub>. *J. Mol. Catal. A* **2006**, *252*, 132–135.
38. Xie, L.J.; Ma, J.F.; Xu, G.J. Preparation of a novel Bi<sub>2</sub>MoO<sub>6</sub> flake-like nanophotocatalyst by molten salt method and evaluation for photocatalytic decomposition of rhodamine B. *Mater. Chem. Phys.* **2008**, *110*, 197–200.
39. Tang, J.W.; Zou, Z.G.; Yin, J.; Ye, J. Photocatalytic degradation of methylene blue on CaIn<sub>2</sub>O<sub>4</sub> under visible light irradiation. *Chem. Phys. Lett.* **2003**, *382*, 175–179.
40. Chu, X.F.; Zheng, C.M. Sulfide-sensing characteristics of MF<sub>2</sub>O<sub>4</sub> (M = Zn, Cd, Mg and Cu) thick film prepared by co-precipitation method. *Sens. Actuators B* **2003**, *96*, 504–508.

41. Chen, C.H.; Liang, Y.H.; Zhang, W.D. ZnFe<sub>2</sub>O<sub>4</sub>/MWCNTs composite with enhanced photocatalytic activity under visible-light irradiation. *J. Alloy. Compd.* **2010**, *501*, 168–172.
42. Qiu, J.X.; Wang, C.Y.; Gu, M.Y. Photocatalytic properties and optical absorption of zinc ferrite nanometer films. *Mater. Sci. Eng. B* **2004**, *112*, 1–4.
43. Du, H.Y.; Luan, J.F. Synthesis, characterization and photocatalytic activity of new photocatalyst CdBiYO<sub>4</sub>. *Solid State Sci.* **2012**, *14*, 1295–1305.
44. Yang, S.X.; Zhu, W.P.; Jiang, Z.P.; Chen, Z.X.; Wang, J.B. The surface properties and the activities in catalytic wet air oxidation over CeO<sub>2</sub>-TiO<sub>2</sub> catalysts. *Appl. Surf. Sci.* **2006**, *252*, 8499–8505.
45. Matuana, L.M.; Balatinecz, J.J.; Sodhi, R.N.S.; Park, C.B. Surface characterization of esterified cellulosic fibers by XPS and FTIR spectroscopy. *Wood Sci. Technol.* **2001**, *35*, 191–201.
46. Izumi, F. Rietan: A software package for the rietveld analysis and simulation of X-ray and neutron diffraction patterns. *J. Crystallogr.* **1985**, *27*, 23.
47. Culea, E.; Pop, L.; Simon, S. Spectroscopic and magnetic behaviour of xGd<sub>2</sub>O<sub>3</sub> (1-x) (Bi<sub>2</sub>O<sub>3</sub> PbO) glasses. *Mater. Sci. Eng. B* **2004**, *112*, 59–63.
48. Soltani, M.; Haddad, S.; Ouennes, K.; Boulegroun, A.; Poulain, M.; Aslan, M.H.; Oral, A.Y. In structural investigations of Sb<sub>2</sub>O<sub>3</sub>-M<sub>2</sub>O (M = Li, Na or K) glasses by the mean of thermal and elastics characterization. *AIP Conf. Proc.* **2012**, *1476*, 87–90.
49. Pillai, S.C.; Kelly, J.M.; McCormack, D.E.; O'Brien, P.; Ramesh, R. The effect of processing conditions on varistors prepared from nanocrystalline ZnO. *J. Mater. Chem.* **2003**, *13*, 2586–2590.
50. Tauc, J.; Grigorovici, R.; Vancu, A. Optical properties and electronic structure of amorphous germanium. *Phys. Status Solidi* **1966**, *15*, 627–637.
51. Luan, J.F.; Wang, S.; Ma, K.; Li, Y.M.; Pan, B.C. Structural property and catalytic activity of new In<sub>2</sub>YbSbO<sub>7</sub> and Gd<sub>2</sub>YbSbO<sub>7</sub> nanocatalysts under visible light irradiation. *J. Phys. Chem. C* **2010**, *114*, 9398–9407.
52. Yang, Y.J.; Luan, J.F. Synthesis, property characterization and photocatalytic activity of the novel composite polymer polyaniline/Bi<sub>2</sub>SnTiO<sub>7</sub>. *Molecules* **2012**, *17*, 2752–2772.
53. Luan, J.F.; Wang, S.; Hu, Z.T.; Zhang, L.Y. Synthesis techniques, properties and applications of polymer nanocomposites. *Curr. Org. Synth.* **2012**, *9*, 114–136.
54. Lachheb, H.; Puzenat, E.; Houas, A.; Ksibi, M.; Elaloui, E.; Guillard, C.; Herrmann, J.M. Photocatalytic degradation of various types of dyes (Alizarin S, Crocein Orange G, Methyl Red, Congo Red, Methylene Blue) in water by UV-irradiated titania. *Appl. Catal. B* **2002**, *39*, 75–90.
55. Vautier, M.; Guillard, C.; Herrmann, J.M. Photocatalytic degradation of dyes in water: Case study of indigo and of indigo carmine. *J. Catal.* **2001**, *201*, 46–59.
56. Shang, X.L.; Li, B.; Li, C.H.; Wang, X.; Zhang, T.Y.; Jiang, S. Preparation and enhanced visible light catalytic activity of TiO<sub>2</sub> sensitized with Benzimidazolone Yellow H3G. *Dyes Pigment.* **2013**, *98*, 358–366.
57. Subash, B.; Krishnakumar, B.; Swaminathan, M.; Shanthi, M. Highly efficient, solar active, and reusable photocatalyst: Zr-loaded Ag-ZnO for Reactive Red 120 dye degradation with synergistic effect and dye-sensitized mechanism. *Langmuir* **2013**, *29*, 939–949.
58. Chen, J.; Poon, C.S. Photocatalytic construction and building materials: From fundamentals to applications. *Build. Environ.* **2009**, *44*, 1899–1906.

59. Ding, H.M.; Sun, H.; Shan, Y.K. Preparation and characterization of mesoporous SBA-15 supported dye-sensitized TiO<sub>2</sub> photocatalyst. *J. Photochem. Photobiol. A* **2005**, *169*, 101–107.
60. Giroto, E.M.; Gazotti, W.A.; Tormena, C.F.; de Paoli, M.A. Photoelectronic and transport properties of polypyrrole doped with a dianionic dye. *Electrochim. Acta* **2002**, *47*, 1351–1357.
61. Marugan, J.; Hufschmidt, D.; Sagawe, G.; Selzer, V.; Bahnemann, D. Optical density and photonic efficiency of silica-supported TiO<sub>2</sub> photocatalysts. *Water Res.* **2006**, *40*, 833–839.
62. Sakthivel, S.; Shankar, M.V.; Palanichamy, M.; Arabindoo, B.; Bahnemann, D.W.; Murugesan, V. Enhancement of photocatalytic activity by metal deposition: Characterisation and photonic efficiency of Pt, Au and Pd deposited on TiO<sub>2</sub> catalyst. *Water Res.* **2004**, *38*, 3001–3008.

© 2014 by the authors; licensee MDPI, Basel, Switzerland. This article is an open access article distributed under the terms and conditions of the Creative Commons Attribution license (<http://creativecommons.org/licenses/by/3.0/>).